Dalton Transactions

PAPER

View Article Online
View Journal | View Issue

Cite this: *Dalton Trans.*, 2014, **43**, 8664

New modular manganese(I) tricarbonyl complexes as PhotoCORMs: *in vitro* detection of photoinduced carbon monoxide release using COP-1 as a fluorogenic switch-on probe†

Sandesh Pai,[a] Maryam Hafftlang,[b] George Atongo,[a] Christoph Nagel,[a] Johanna Niesel,[a] Svetlana Botov,[c] Hans-Günther Schmalz,[c] Benito Yard[b] and Ulrich Schatzschneider*[a]

Received 23rd January 2014,
Accepted 1st March 2014

DOI: 10.1039/c4dt00254g

www.rsc.org/dalton

Five manganese(I) tricarbonyl complexes of the general formulae $[Mn(bpea^{N=CHC6H4R})(CO)_3]PF_6$ and $[Mn(bpea^{NHCH2C6H4R})(CO)_3]PF_6$ based on the tridentate bis(pyrazolyl)ethylamine (bpea) ligand, each containing a pendant 4-substituted phenyl group with R = H, I, and C≡C–H, were synthesized and fully characterized, including X-ray structure analysis for three compounds. All complexes are stable in the dark in aqueous buffer for an extended period of time. However, CO-release could be triggered by illumination at 365 nm, establishing these compounds as novel photoactivatable CO-releasing molecules (PhotoCORMs). The influence of the imine *vs.* amine group in the ligands on the electronic structure and the photophysical behavior was investigated with the aid of DFT and TDDFT calculations. Solution IR studies on selected compounds allowed identification of intermediates resulting from the photoreaction. Finally, light-induced CO release from a model compound was demonstrated both in PBS buffer and *in vitro* in human umbilical vein endothelial cells (HUVECs) using COP-1 as a fluorescent switch-on probe.

Introduction

Carbon monoxide is now well-established as one of the three major small signalling molecules in higher organisms, including humans.[1–4] It is enzymatically generated by haem degradation by the constitutive (HO-2) and inducible (HO-1) isoforms of haem oxygenase (HO), also leading to the formation of ferrous iron and biliverdin, with the latter further converted to bilirubin.[5–8] Its main physiological role is in vasodilation and response to oxidative stress, but the concentration-dependent switch between cytoprotective and cytotoxic activity is also increasingly explored now in the context of potential therapeutic applications.[9–12] There are some devices available which allow for a controlled application of CO gas mixtures to patients, but in addition to the general safety issues associated with the use of an odorless gaseous compound which is highly toxic when overdosed, a major problem of inhalative application is that the final attainable cellular concentration is determined by the partition ratio of CO in the lungs, body fluids, and tissues, which are fixed values. Therefore, over the last decade, carbonyl compounds have been explored as solid, easy-to-handle prodrugs for carbon monoxide delivery to biological systems.[13] Most of these CO carrier systems, collectively referred to as *CO-releasing molecules* (CORMs),[14–17] are based on transition metal carbonyl complexes, although a few main group carbonyl compounds[18–20] and, more recently, purely organic systems have been explored.[21,22] In addition to ligand exchange reactions with medium,[23] there are also other trigger mechanisms to initiate the CO release. These include enzymatic cleavage of remote bonds by esterases and phosphatases in enzyme-triggered CORMs (ET-CORMs),[24–27] magnetic heating of CORM-loaded maghemite nanoparticles,[28] and probably most prominently, light-induced liberation of carbon monoxide from the metal coordination sphere in photoactivatable CO-releasing molecules (PhotoCORMs).[29–31] Iron,[32–35] molybdenum,[36] tungsten,[37] rhenium,[38] and manganese[39–46] carbonyl complexes have received particular attention in this context. While most of these systems are relatively simple, low-molecular weight compounds, more recently, conjugation of CORMs to

[a]*Institut für Anorganische Chemie, Julius-Maximilians-Universität Würzburg, Am Hubland, D-97074 Würzburg, Germany.*
E-mail: ulrich.schatzschneider@uni-wuerzburg.de
[b]*V. Medizinische Klinik, Universitätsmedizin Mannheim, Theodor-Kutzer-Ufer 1-3, D-68167 Mannheim, Germany*
[c]*Institut für Organische Chemie, Universität zu Köln, Greinstr. 4, D-50939 Köln, Germany*

†Electronic supplementary information (ESI) available. CCDC 976263, 976264 and 976267. For ESI and crystallographic data in CIF or other electronic format see DOI: 10.1039/c4dt00254g

macromolecular and nanoparticle carrier systems has also received more and more attention, in order to achieve additional control of CORM tissue accumulation and CO biological activity. In addition to soft peptide,[36,47,48] dendrimer,[49] and polymer[50] conjugates and CORM-loaded micelles,[51] hard CORM-modified nanomaterials have been reported,[52,53] including those in which the CO is loaded into a porous material[54] instead of surface decoration of nanoparticles with molecular metal-carbonyl groups. Such polyfunctional CO delivery systems would significantly benefit from a modular ligand design, allowing facile introduction of different functional groups onto the periphery, which can undergo mild, bioorthogonal coupling reactions[55–58] with macromolecular and nanoscale carriers. Since the modified tris(pyrazolyl)-methane (tpm)[47,52,53] and 2,2′-bipyridine (bpy)[36,49,59] ligands used in our previous studies do not allow such a modular approach, we have recently started to explore the use of a bis(pyrazolyl)ethylamine (bpea)-based ligand system, which offers an easy, flexible, and modular introduction of reactive functional groups for further bioconjugation *via* condensation with *para*-substituted benzaldehydes, leading to either imine- or amine-containing *N*,*N*,*N*-chelators, depending on a subsequent reduction step or not. In the present work, we would like to report on the CO-release properties of manganese(I) tricarbonyl complexes of the parent bpea ligand as well as iodo- and alkyne-functionalized derivatives thereof, prepared for potential use in Sonogashira and CuAAC "click" reactions. Furthermore, it was the aim of our study to explore the utility of the recently reported fluorescent COP-1 probe[60–62] to monitor the photoinduced CO-release from our novel PhotoCORMs in living human umbilical vein endothelial cells (HUVECs) to confirm that carbon monoxide delivery using these compounds indeed works in a complex biological environment.

Results and discussion

Synthesis and characterization

Five new functionalized ligands **9–13** based on the bis(2-pyrazolyl)ethylamine (bpea) moiety were synthesized by condensation of amine **5** with *para*-substituted benzaldehydes **6–8** (Scheme 1 and Scheme S1†). Three ligands **9–11** incorporate an imine backbone with a pendant 4-substituted phenyl group, in which R = H, I, or C≡C–H, with the latter two providing a handle for further bioconjugation *via* Sonogashira or CuAAC "click" reactions. Reduction of the imines **9–10** with sodium borohydride gave ligands **12–13** with the more stable amine group. All five ligands were obtained in good yields of 70–80%. The facial manganese(I) tricarbonyl complexes **14–18** (Fig. 1) were obtained in moderate to good yields by reaction of ligands **9–13** with manganese pentacarbonyl bromide in acetone at reflux under a dinitrogen atmosphere with exclusion of light (Scheme S2†). Prominent IR vibrational bands of **14–18** are listed in Table 1. Compared to the free imine ligands **9–11**, the C=N stretching vibrations are shifted to lower wavenumbers upon coordination to the Mn(I) center in **14–16**.

Furthermore, all complexes show two intense bands at about 1930 and 2040 cm^{-1}, which are assigned to the antisymmetrical and symmetrical C≡O stretching vibrations of the metal tricarbonyl moiety, respectively, see Fig. 2 for a selected example. As expected due to the large number of intervening bonds, no influence of the *para*-substituent on the phenyl ring on their position is observed.

The ^{1}H NMR chemical shifts of ligands **9–13** and their corresponding complexes **14–18** are collected in Table S1.† The signal of the methine proton shifts from about 6.8 ppm in the imine ligands **9–11** to 7.8 ppm for complexes **14–16**, while a slightly smaller shift from 6.5 ppm in the amine ligands **12–13** to 7.4 ppm for complexes **17–18** was observed upon coordination to the Mn(I) center. Furthermore, the imine proton shifts from 8.2 ppm in ligands **9–11** to 9.4 ppm for complexes **14–16** (Fig. S1–S3†). Only a broad singlet appears at 5.6 ppm due to the amine proton in **17–18** (Fig. S4, S5†). The two protons of the methylene group adjacent to both the

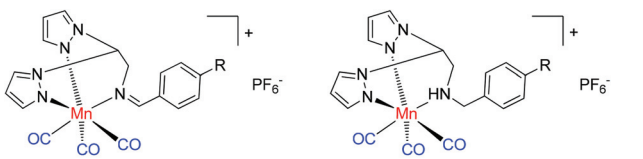

14, R = -H
15, R = -I
16, R = -C≡CH

17, R = -H
18, R = -I

Fig. 1 *fac*-Manganese(I) tricarbonyl bpea complexes **14–18**.

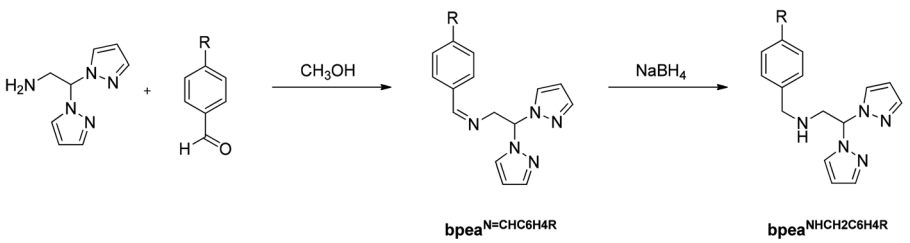

5

6, R = -H
7, R = -I
8, R = -C≡CH

9, R = -H (73%)
10, R = -I (88%)
11, R = -C≡CH (72%)

12, R = -H (78%)
13, R = -I (72%)

Scheme 1 Synthesis of ligands **9–13**.

Table 1 Prominent IR vibrational band positions (in cm^{-1}) of ligands **9–13** and complexes **14–18**

	C═N	C≡O$_{antisym}$	C≡O$_{sym}$
9	1649	—	—
10	1644	—	—
11	1641	—	—
12	—	—	—
13	—	—	—
14	1625	1932	2040
15	1624	1931	2043
16	1633	1930	2041
17	—	1939	2045
18	—	1928	2041

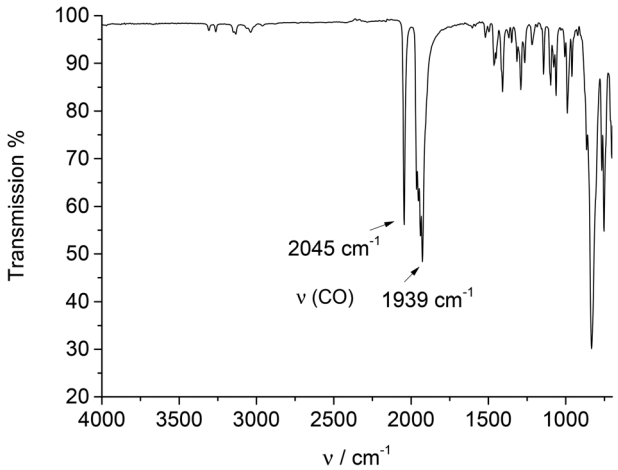

Fig. 2 ATR IR spectrum of [Mn(bpea^{NHCH2C6H5})(CO)$_3$]PF_6 **17**, showing the symmetrical and antisymmetrical C≡O stretching vibrations at 2045 and 1939 cm^{-1}.

coordinated amine and the methine give rise to individual signals at 3.1 and 3.5 ppm, respectively, due to the diastereotopic environment generated by metal coordination of the amine, and both are further split by coupling to the neighboring CH and NH protons. In contrast, in the free ligands **12–13**, these give rise to only a single doublet at around 3.7 ppm. In the imine compounds, this signal is much less sensitive to a coordination-induced shift and for both ligands **9–11** and complexes **14–16** appears at about 4.6 ppm.

Molecular structures of the complexes

Single crystals suitable for X-ray structure analysis were obtained by slow diffusion of *n*-hexane into acetone solutions of **15**, **17**, and **18**. Crystallographic parameters are listed in Table 2 and Table S2.† Selected bond distances and angles of the complexes are collected in Table 3 and Table S3.† Molecular structures are shown in Fig. 3 and 4 as well as Fig. S6.† In each case, the three carbonyl ligands are coordinated to the Mn(I) center in a facial manner. Three nitrogen atoms of the tridentate bpea ligand, two from the pyrazol groups and one from the imine/amine, are located opposite to the CO ligands to give an approximate C_{2v} symmetry of the $Mn(CO)_3N_3$ core, which is however broken by the orientation of the substituents

Table 2 Crystallographic parameters for **15** and **18**

Compound	**15**	**18**
Empirical formula	$C_{18}H_{14}F_6IMnN_5O_3P$	$C_{21}H_{22}BrIMnN_5O_4$
Formula weight	675.15	670.19
Dimensions (mm)	0.30 × 0.25 × 0.15	0.30 × 0.10 × 0.10
Crystal system	Monoclinic	Triclinic
Space group	$P2(1)/n$	$P\bar{1}$
a (Å)	14.7315(7)	9.8908(3)
b (Å)	11.1201(3)	11.9141(4)
c (Å)	15.6814(7)	12.1870(3)
α (°)	90	98.487(2)
β (°)	116.031(6)	110.618(3)
γ (°)	90	106.055(3)
V (Å^3)	2308.27(19)	1242.87(6)
Z	4	2
ρ_{calc} (g cm^{-3})	1.943	1.791
T (K)	113(2)	113(2)
μ (mm^{-1})	2.059	3.417
λ (Å) (Mo K_α)	0.71073	0.71073
$2\Theta_{max}$ (°)	25.00	25.00
Reflections measured	7728	13 673
Unique refl./$[I > 2\sigma(I)]$	4066/3435	4376
Data completeness	0.999	0.998
Variables	316	302
R $(I \geq 2\sigma(I))$	0.0301	0.0200
wR $(I \geq 2\sigma(I))$	0.0643	0.0460
Largest difference map peak/hole in e Å^{-3}	0.802/−0.463	0.593/−0.291
Goodness of fit (GOF)	1.026	0.954

Table 3 Selected bond lengths (Å) and angles (°) for complexes **15** and **18**

	15	**18**
Mn1–C1	1.812(3)	1.805(2)
Mn1–C2	1.822(4)	1.801(2)
Mn1–C3	1.804(4)	1.818(2)
Mn1–N1	2.091(2)	2.133(2)
Mn1–N3	2.042(3)	2.036(2)
Mn1–N5	2.042(3)	2.035(2)
C1–O1	1.144(4)	1.153(3)
C2–O2	1.141(4)	1.151(3)
C3–O3	1.147(4)	1.146(3)
C5–N2	1.451(4)	1.456(3)
C5–N4	1.454(4)	1.453(3)
C4–C5	1.510(4)	1.519(3)
C4–N1	1.479(4)	1.484(3)
N1–C12	1.289(4)	1.501(3)
C1–Mn1–N1	175.09(13)	174.30(8)
C2–Mn1–N3	178.48(13)	177.90(9)
C3–Mn1–N5	176.86(12)	178.03(9)
(Mn1–N1–C4–C5)–(N1–C12–C13)	8.1°	48.7°
(N1–C12–C13)–(C13–C14–C15–C16–C17–C18)	9.7°	93.7°

on the sp^3 amine nitrogen atom in **17** and **18**. The effect of the imine *vs.* amine ligation is also clearly reflected in the Mn1–N1 bond distance, which is 2.091(2) Å in **15** but extended by about 0.04 Å to 2.133(2) Å in **18**. The other parameters, in particular the Mn–C, Mn–N$_{pyrazole}$, and C≡O bond distances, show much less variation between the compounds and generally do not deviate by more than 0.02 Å from **15** to **18**. The N1–C12 bond length is 1.289(4) Å in imine complex **15** and 1.501(3) Å in amine compound **18**. Bond angles around the metal center are close to 90° and 180°, respectively, as expected

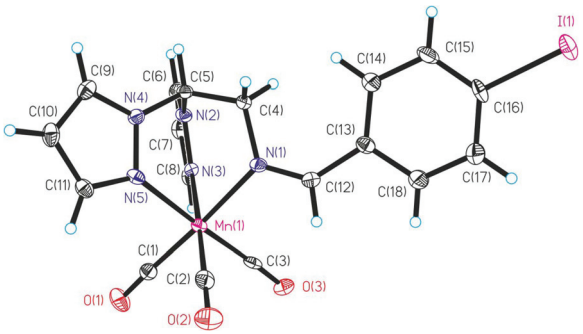

Fig. 3 Molecular structure of the cationic unit of **15** with ellipsoids drawn at the 50% probability level. The hexafluorophosphate counterion is not shown for clarity.

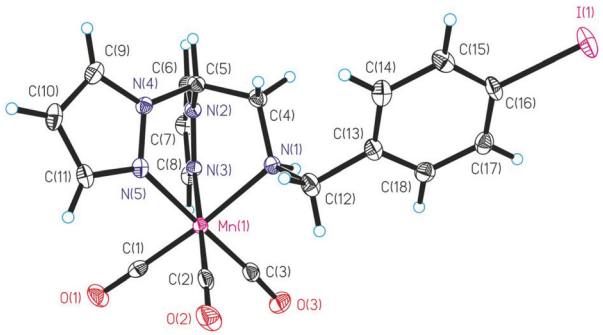

Fig. 4 Molecular structure of the cationic unit of **18** with ellipsoids drawn at the 50% probability level. The bromide counterion and a solvate acetone molecule are not shown for clarity.

for a near-octahedral coordination environment. The most prominent difference between the imine and amine complexes is, however, the orientation of the phenyl ring relative to the bis-(pyrazolyl) core. In imine compound **15**, it is essentially located in the mean plane intersecting the N3–Mn1–N5 and C2–Mn1–C3 angles, as defined by Mn1, N1, C4, and C5, and only slightly distorted relative to the C═N group, with a (Mn1–N1–C4–C5)–(N1–C12–N13) angle of 8.1° and a (N1–C12–C13)–phenyl angle of 9.7°. In amine complex **18**, on the other hand, the sp^3 configuration of N1 leads to significantly expanded dihedral angles of 48.7° and 93.7° for the orientation of these atoms. The unsubstituted parent compound **17** shows a similar effect, with the two independent molecules in the unit cell having essentially identical parameters, with the exception of the relative orientation of the phenyl ring (Table S3†).

Electronic absorption spectra and photolysis of the complexes

The UV/Vis absorption spectra of complexes **14–18** were recorded in dimethylsulfoxide and are shown in Fig. 5. For all five complexes, a broad maximum centered at around 350 nm with an extinction coefficient of about 2500–5000 M^{-1} cm^{-1} is observed (Table 4), which is assigned to a metal-to-ligand charge transfer transition (*vide infra*). The intensity of this band is somewhat smaller for the amine *vs.* imine compounds, and for the former complexes also show less variation with the

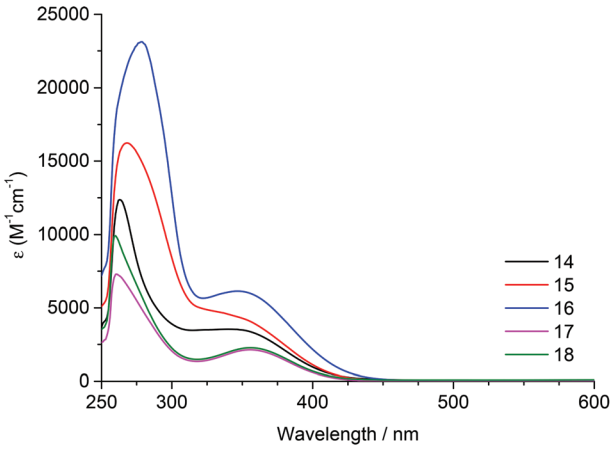

Fig. 5 UV/Vis absorption spectra of **14–18** in DMSO.

Table 4 Absorption maxima and molar extinction coefficient of complexes **14–18**

Compound	λ_{max} [nm]	$\varepsilon_{\lambda_{max}}$ [M^{-1} cm^{-1}]	$\varepsilon_{365\ nm}$ [M^{-1} cm^{-1}]
14	341	3460 ± 60	3005 ± 55
15	348	4410 ± 60	3550 ± 40
16	347	5500 ± 310	5495 ± 95
17	355	2135 ± 80	2020 ± 85
18	356	2275 ± 80	2155 ± 65

nature of the *para*-substituent on the phenyl ring, which is thought to be due to a decrease in electronic communication with the metal center for $NHCH_2$ *vs.* N═CH. The stability of the compounds was also studied in aerated DMSO solution. They did not show any change in absorbance when kept in the dark over a course of 14 h, as shown for **17** as an example in Fig. 6. However, illumination at 365 nm using a UV lamp leads to a pronounced decrease in absorption (Fig. S7†). A plateau

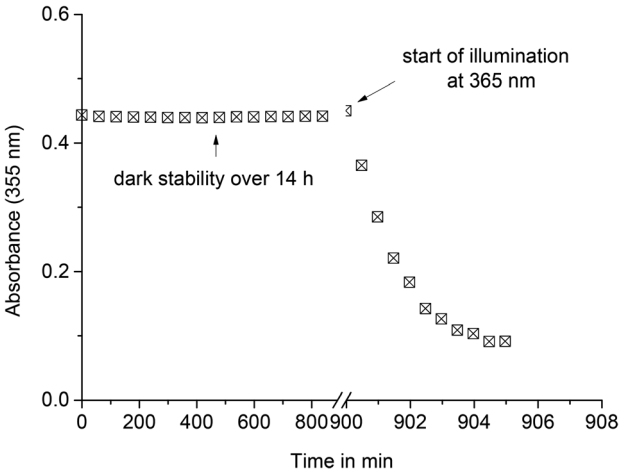

Fig. 6 Changes in the absorbance at 355 nm of **17** upon incubation in dimethylsulfoxide in the dark for the initial 14 h and during subsequent photolysis of the same solution with an UV lamp at 365 nm. See Fig. S7† for the full spectral traces.

value was reached after a couple of minutes, with the half-life determined as 1.5 min from proper fitting of the data. When the same experiment was repeated on **17** with LED illumination at 410 nm, essentially the same spectral changes are observed (data not shown), but the half-life is significantly extended to 52 min, which is due to the much lower extinction coefficient at this wavelength (see Fig. 5).

Photoinducible CO release and quantum yield measurements

The dark stability and photoactivated release of CO from complexes **14–18** was assessed with the standard myoglobin assay.[63,64] In these experiments, a freshly prepared concentrated solution of metal complex in dimethylsulfoxide was added to a buffered solution (PBS, pH 7.4) of horse skeletal myoglobin (Mb), which was reduced with excess sodium dithionite under dinitrogen in the dark. When kept in the dark for up to 14 h under the conditions described above, none of the compounds **14–18** induced any spectral changes in the Q-band region of myoglobin, as shown for **17** in Fig. 7 as an example, thus establishing them as dark-stable CORM prodrugs. However, when illuminated at 365 nm, the absorption of Mb at 557 nm decreased and the typical peaks of MbCO at 540 and 577 nm grew in intensity with increasing illumination time (Fig. S8†). The amount of MbCO formed at the plateau level (Fig. 8) was calculated using the published extinction coefficient of MbCO [$\lambda_{540\ nm}$ = 15.4 $(mM)^{-1}$ L^{-1}].[65] The half-lives of CO release, equivalents of carbon monoxide liberated from complexes **14–18**, and their reaction quantum yields determined at 365 nm ($\Phi_{365\ nm}$) are listed in Table 5.

All five complexes release about two equivalents of CO under the conditions of the myoglobin assay at 365 nm illumination. However, the half-lives of the imine complexes **14–16** are slightly shorter than those of the amine compounds **17–18** at 19–22 min *vs.* 26–29 min. To investigate the effect of lower energy photoactivation, complex **17** was also studied using 410 nm illumination from a LED array. While there is essentially no change in the number of CO ligands released at this excitation wavelength (2.1 eq. at 365 nm *vs.* 2.4 eq. at 410 nm), the half-life of CO release is significantly extended to 132 min at 410 nm due to the lower absorption at this wavelength. The reaction quantum yields of complexes **17–18** are slightly lower than those of the imine compounds **14–16**. Still, the Φ values are much lower than those reported for $[Mn(CO)_3(tpa)]ClO_4$ and $[Mn(CO)_3(dpa)]Br$[66] at similar wavelengths and in the order of 10^{-3}, which is due to the internal shielding by the horse skeletal myoglobin absorption at the excitation wavelength of 365 nm. Nevertheless, the present data establish manganese(I) tricarbonyl complexes **14–18** as a new family of Mn-based photoactivatable CO-releasing molecules (PhotoCORMs) with good dark stability and modular synthesis, facilitating further modification and bioconjugation.

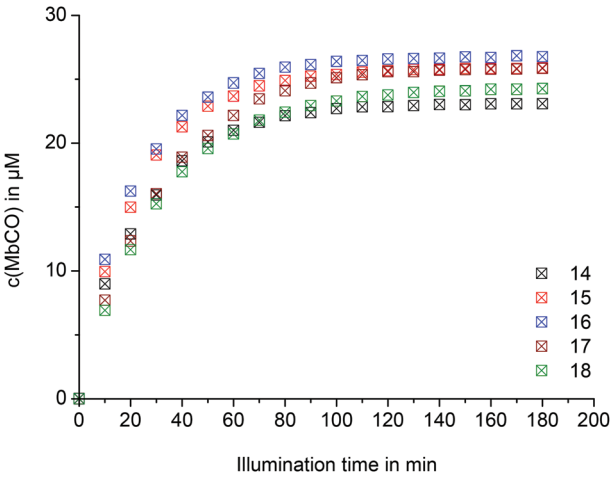

Fig. 8 Comparison of the amount of MbCO (in µM) formed with increasing illumination time of a solution of complex **14–18** (10 µM) and myoglobin (60 µM) in 0.1 M PBS pH 7.4 at 365 nm.

DFT and TDDFT calculations

To obtain a more detailed picture of the effect of the imine *vs.* amine group in the ligands on the photophysical and photochemical properties of the title compounds and to assign the

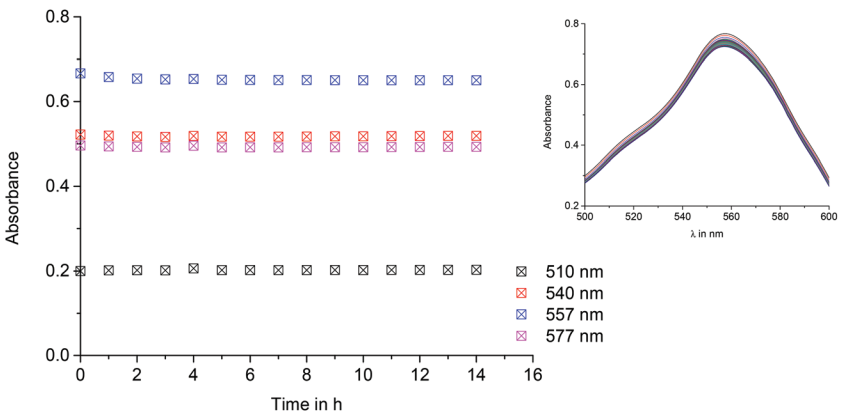

Fig. 7 Absorbance values at four different wavelengths in the Q-band region of myoglobin (60 µM) upon incubation with complex **17** (10 µM) in the dark for up to 14 h in 0.1 M PBS at pH 7.4 with sodium dithionite (10 mM) under a dinitrogen atmosphere and (inset) UV/Vis absorption spectra recorded at different time points during the dark incubation.

Table 5 CO-release data and reaction quantum yield values at 365 nm for **14–18**

Compound	Conc. of MbCO [μM]	Equiv. of CO released	Half-life, $t_{1/2}$ [a] [min]	Rate constant k_{CO} [b] [s^{-1}]	Reaction quantum yield ($\Phi_{365\ nm}$ [c])
14	22.5 ± 0.3	2.3 ± 0.1	21.6 ± 0.3	0.00642	$(5.9 \pm 0.2) \times 10^{-3}$
15	24.8 ± 0.8	2.5 ± 0.1	21.3 ± 0.5	0.01060	$(6.3 \pm 0.4) \times 10^{-3}$
16	23.2 ± 0.2	2.3 ± 0.1	18.5 ± 0.2	0.01208	$(6.6 \pm 0.1) \times 10^{-3}$
17	20.7 ± 0.3	2.1 ± 0.1	25.8 ± 0.2	0.00783	$(4.4 \pm 0.2) \times 10^{-3}$
18	21.3 ± 0.3	2.1 ± 0.1	28.7 ± 0.8	0.00745	$(4.3 \pm 0.2) \times 10^{-3}$

[a] Under the conditions of the myoglobin assay. [b] Determined in DMSO solution. [c] Calculated using a photon flux of the UV lamp of $(2.82 \pm 0.05) \times 10^{-8}$ Einstein s^{-1}.

C≡O vibrations of intermediate species resulting from photo-induced carbon monoxide release from the metal coordination sphere, DFT and TDDFT calculations were carried out on imine $[Mn(bpea^{N=CHC6H5})(CO)_3]^+$ **A** and amine $[Mn(bpea^{NHCH2C6H5})(CO)_3]^+$ **B**, generated from the X-ray structures of **15** and **18**, respectively, by removal of counterions and solvate molecules as well as replacement of the iodo group by hydrogen in the *para*-position of the phenyl ring. The ORCA program package with the RI-BP86 (geometry optimization and calculation of vibrational frequencies) or RIJCOSX-B3LYP functionals (TDDFT) and a TZVP basis set on all atoms was used in both cases, taking into account the DMSO solvent with the COSMO model. As already observed in DFT studies of related manganese(I) tricarbonyl complexes using a similar model chemistry,[49] the deviations between calculated bond distances and angles from those obtained by X-ray crystallography are very small and do not exceed 2.5% as averaged over all parameters (Table S4†).

No imaginary frequencies were found among the calculated vibrational modes, establishing the geometries obtained as minimum structures, but due to significant deviation from the experimental values they had to be scaled by a factor of 1.036, which leads to an excellent agreement with all deviations below 1% or, in absolute terms, less than 20 cm^{-1}. It should be noted that this scaling factor deviates from the ones reported in some literature, but was obtained from a specific training set based on metal carbonyl compounds. A comparison of calculated and experimental vibrations is presented in Table 6 together with the assignment of the major modes. The broad antisymmetrical C≡O stretch could not be resolved in the two contributions in the experimental ATR IR spectra. As observed previously,[49] the antisymmetrical C≡O stretches are underestimated by a maximum of about 20 cm^{-1}, while the symmetrical one is overestimated by about the same value when scaled as above. To investigate the influence of the imine *vs.* amine group on the electronic structure of the title compounds, TDDFT calculations were carried out on the minimum geometries and the first 45 singlet excited states obtained this way (Table 7). As expected for a Mn(I) center with a low-spin $3d^6$ electronic configuration, the HOMO to HOMO−2 orbitals are essentially of metal d character in **A** as well as **B**, and well-separated by 0.79 and 0.45 eV, respectively, from the next lowest occupied orbital, which is of π phenyl character (Tables S5 and S7†). The LUMO is of mixed phenyl/imine character in **A**, but centered on the two pyrazole groups in **B**. Further unoccupied orbitals are either of π*(pyrazole), π*(phenyl), or π*(CO) character. The low-energy states of relevant oscillator strength are all of MLCT character (Table 7). However, while those in the range of 300–350 nm are from the manganese to the pyrazoles for both **A** and **B**, the imine compound **A** is predicted to show an additional Mn→phenyl/imine MLCT at around 470 nm. Presumably, conjugation of the N=CH group with the phenyl ring lowers the energy of one of the π* orbitals of this group by about 2 eV, making it the LUMO and leading to its significant contribution to the lowest-energy state. Only below about 300 nm, the difference densities show additional LLCT and ILCT transitions (Tables S6 and S8†). The manganese→pyrazole MLCT transitions close to the excitation wavelength of 365 nm will decrease the metal electron density in the excited state, which results in a weakening of the back-donation to the CO π* orbitals and subsequently facilitates M–CO bond breaking, resulting in liberation of the carbon monoxide from the metal coordination sphere, as has been demonstrated for other manganese-based PhotoCORMs before.[41,49]

Table 6 Comparison of major experimental and scaled calculated vibrational frequencies for **14** and **17** *vs.* **A** and **B**. The deviation from the experimental values is given in parentheses (all in cm^{-1})

Mode	**14** exp.	**A** calc.	**17** exp.	**B** calc.
ν(CH=N)	1625	1605 (−20)	—	—
$\nu_{antisym1}$(C≡O)	1932	1929 (−3)	1939	1922 (−17)
$\nu_{antisym2}$(C≡O)	1932	1930 (−2)	1939	1928 (−11)
ν_{sym}(C≡O)	2040	2059 (+19)	2045	2066 (+21)

CO release studied by solution IR spectroscopy

In order to follow the CO release upon photoactivation, solutions of **14** and **17** were prepared in DMSO. The sample solution was filled in a liquid IR cell and was illuminated at 365 nm for fixed time intervals after which IR spectra were recorded. The carbonyl vibrational region of the IR spectra is shown in Fig. 9 and Fig. S9† for compounds **17** and **14**, respectively. The two bands at 2038 and 1939 cm^{-1}, which are typical for *fac*-$Mn(CO)_3$ complexes, decrease in intensity upon illumination while three to four new bands appear in the region between 1640 and 1900 cm^{-1}. Interestingly, these signals persist even after prolonged illumination, which is not the case with other related compounds such as

Table 7 Energies (in nm), oscillator strength (f_{osc}), main orbital contributions, and the type of transition involved in the most important singlet excitations for imine **A** and amine **B** calculated with TDDFT

A

State[a]	λ (nm)	f_{osc}	Main transitions[b]	Type of transition
2	469.3	0.2602	102→103 (95%)	MLCT Mn→phenyl + imine
4	350.0	0.0168	102→104 (92%)	MLCT Mn→pyrazole
5	329.2	0.0528	101→104 (71%)	MLCT Mn→pyrazole
			102→105 (22%)	
8[c]	296.7	0.1258	102→105 (54%)	MLCT Mn→pyrazole(+phenyl)
9[c]	299.4	0.0941	101→105 (83%)	MLCT Mn→pyrazole
11[c]	304.4	0.1377	97→103 (55%)	LLCT phenyl→pyrazole
			98→103 (43%)	
13	264.7	0.0850	102→107 (75%)	MLCT Mn→CO
15	260.6	0.0362	101→108 (84%)	MLCT Mn→CO
18	258.5	0.4138	97→103 (38%)	ILCT phenyl→phenyl
			98→103 (41%)	

B

State[a]	λ (nm)	f_{osc}	Main transitions[b]	Type of transition
1	343.0	0.0110	102→104 (84%)	MLCT Mn→pyrazole
2	337.2	0.0781	103→104 (82%)	MLCT Mn→pyrazole
4	304.8	0.1017	103→105 (75%)	MLCT Mn→pyrazole
5	295.4	0.0660	102→105 (70%)	MLCT Mn→pyrazole
7	280.6	0.0127	101→105 (62%)	MLCT Mn→pyrazole
8	276.2	0.0446	101→105 (21%)	MLCT Mn→pyrazole + phenyl
			103→106 (48%)	
10	261.0	0.0545	102→108 (70%)	MLCT Mn→CO
13	253.5	0.0190	100→104 (57%)	MLCT/LLCT phenyl→pyrazole

[a] Only strong transitions with an oscillator strength >0.01 in the 250–600 nm range are reported. [b] Only contributions >20% are listed. [c] The reversed order is due to the states experiencing a different degree of solvent shift.

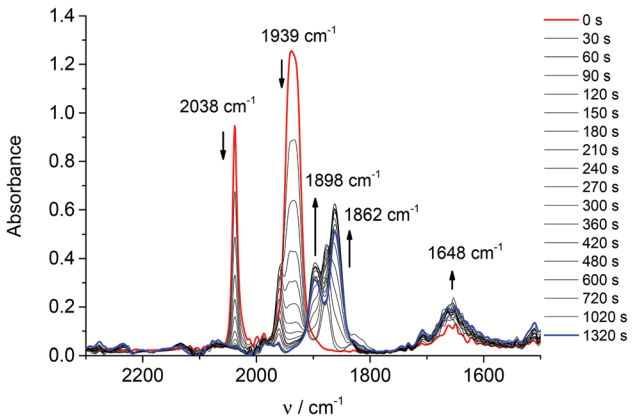

Fig. 9 Spectral changes in the solution IR of **17** (9 mM solution in DMSO) upon illumination (0–1320 s) at 365 nm. The red trace was recorded on a freshly prepared solution before the start of the illumination whereas the blue trace shows the final spectrum recorded after about 22 min of illumination.

$[Mn(CO)_3(tpm)]^+$, $[Mn(CO)_3(tpa\text{-}\kappa^3N)]^+$, and $[Mn(CO)_3(tpp)]^+$.[67] The two signals growing at 1898 and 1862 cm^{-1} for **17** are indicative of a *cis*-$Mn(CO)_2$ moiety remaining after the release of the first equivalent of carbon monoxide, while the 1648 cm^{-1} band appears at the same position as found in imine ligands **9–11** for the C=N stretching vibration. This result contrasts with the release of two equivalents of carbon monoxide observed under the conditions of the myoglobin assay (*vide supra*).

To assist in the assignment of the species resulting from the photolysis, DFT calculations were carried out to obtain the vibrational signature of potential products and intermediates (Table 8). The general validity of this approach was previously demonstrated by comparison of optimized geometries to those of the X-ray structural data of **14** and **17**. Two isomers were examined for each CO release step, depending on whether the CO liberated originates from a position *trans* to a pyrazole or *trans* to the amine/imine group (Fig. 10). In line with previous

Table 8 Scaled calculated vibrational frequencies for potential products **C** to **F** resulting from the prolonged photolysis of imine **14** and amine **17** at 365 nm with differences to experimental values in round brackets (all in cm^{-1})

Mode	C	C′	D[a]	D′
ν(CH=N)	1560 (−89)	1554 (−95)	—	1629 (−20)
$\nu_{antisym}$(C≡O)	1862 (+2)	1863 (−2)	—	—
ν_{sym}(C≡O)	1935 (+39)	1940 (+44)	—	1848 (+24)[b]
Mode	**E**	**E′**	**F**	**F′**
$\nu_{antisym}$(C≡O)	1846 (−16)	1835 (−27)	—	—
ν_{sym}(C≡O)	1935 (+37)	1919 (+21)	1825[b,c]	1826[b,c]

[a] Could not be converged in the low-spin state. [b] Monocarbonyl species, only one C≡O vibrational mode. [c] Not observed, probably covered by remaining signals of the starting material.

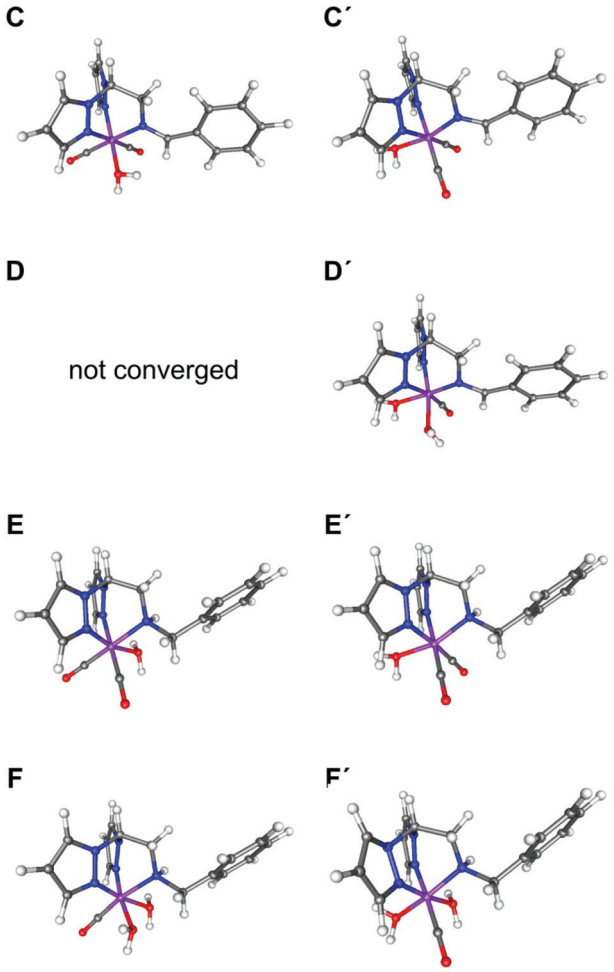

Fig. 10 Structure of the cationic unit of iCORM intermediates **C**–**F** optimized with BP86 after subsequent removal of carbonyl ligands and replacement with one or two solvent water molecules. Color coding: carbon (grey), hydrogen (white), nitrogen (blue), oxygen (red), manganese (magenta).

studies, the octahedral coordination sphere of the manganese center was retained and departed CO was replaced by water molecules as models for solvent. As evident from Table 8, using this methodology, it is not possible to conclusively decide between these two cases. However, the first intermediate is clearly identified as a *cis*-manganese dicarbonyl, and at least in the case of the imine complex **14**, also some amount of monocarbonyl seems to form after extended photolysis (Fig. S9†).

In vitro detection of CO release using the COP-1 fluorogenic switch-on probe

Very recently, the groups of Chang and He reported on fluorescence-based molecular probes for the detection of carbon monoxide in complex biological systems.[60–62] We were particularly interested in the application of COP-1, since it is based on a small-molecule system composed of a BODIPY switch-on fluorescent dye coupled to a cyclometalated dimeric palladium unit, which is cleaved upon reaction with carbon monoxide. The COSer system from the group of He, on the other hand, originates from a modified protein and thus is expected to have much less general applicability. Since both systems have so far only been evaluated using CO gas and CORM-3 as the carbon monoxide source, we were particularly interested to validate whether a response to photoinduced carbon monoxide release from our PhotoCORMs could also be detected. Initially, the COP-1 response was examined in PBS buffer in the presence and absence of light. A dose-dependent increase in fluorescence signal was observed when increasing amounts of PhotoCORM **17** (0–100 μM) were added to COP-1 (10 μM in PBS) followed by photoactivation at 365 nm for 30 min while in the non-illuminated sample, the fluorescence intensity of the mixture remained at the basal level (Fig. 11).

Importantly, even at a 1 : 10 molar ratio of COP-1 to PhotoCORM **17**, which translates to a 1 : 20 molar ratio of COP-1 to labile CO, if one assumes that only two out of the three carbonyl ligands are released from the metal coordination sphere, the signal was still not fully saturated and a non-linear response of COP-1 fluorescence with increasing CO concentration was observed.

To check whether the light-triggered release of carbon monoxide from **17** could also be detected by COP-1 in living cells, human umbilical vein endothelial cells (HUVECs) were incubated in microtiter plates with COP-1 (10 μM) in PBS followed by addition of PhotoCORM **17** (100 μM) in the dark. The cell cultures were then exposed to 365 nm light for 30 min, while a control experiment was performed under exactly the same conditions, but without illumination. Further controls included phosphate buffer saline (PBS) only as well as COP-1 and sodium hexafluorophosphate in the same buffer, both in the presence and absence of UV light. At the end of the experiment, the supernatant and the cell-containing phase were separated and individually assessed. The molecular probe

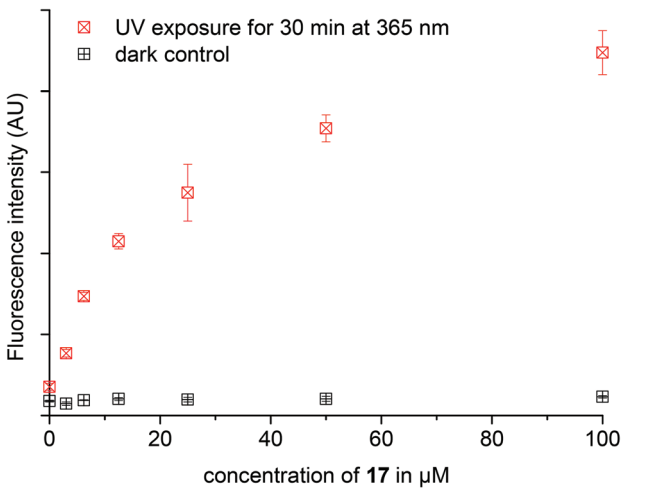

Fig. 11 Dose-dependent fluorescence response of 10 μM COP-1 in PBS to photoinduced release of CO from increasing amounts of **17** (data points shown at 0, 3, 6, 12.5, 25, 50, and 100 μM). Fluorescence intensity was measured at an emission wavelength, λ_{em} = 510 nm with λ_{ex} = 475 nm. The data are expressed as mean fluorescence intensity ± SD with experiments performed in quadruplicate.

remaining in the supernatant only shows a very weak fluorescence both in the dark control and upon illumination at 365 nm for 30 min (Fig. 12a, 2nd column). The same is also true for complex **17** alone (Fig. 12a, 3rd column). Furthermore, sodium hexafluorophosphate as the source of the counter ion and a mix of COP-1 and $NaPF_6$ were also examined for background signal but found to be non-emissive (Fig. 12a, 5th and 6th columns). The same is also true for a mixture of COP-1 (10 μM) and compound **17** (100 μM) in PBS when kept in the dark (Fig. 12a, 4th column). Only the combination of added metal carbonyl complex **17** and illumination led to a significant, about 15-fold increase in fluorescence intensity (Fig. 12a, 4th column), while under all other conditions, the emission remained at essentially baseline level. A similar trend was observed with the cell-based fraction, but the increase for the illuminated *vs.* non-illuminated sample was only about 5-fold higher compared to the controls, and thus significantly smaller than observed in the supernatant. This could be due to impaired cellular uptake of either the COP-1 probe or the metal complex, or both, or some kind of deactivation or quenching process. Thus, although COP-1 is very important as one of the first *in vitro* probes for carbon monoxide and was also demonstrated here to allow detection of light-induced CO release from PhotoCORMs, clearly more improved and sensitive derivatives thereof are urgently needed as tools for the study of small-molecule signalling.

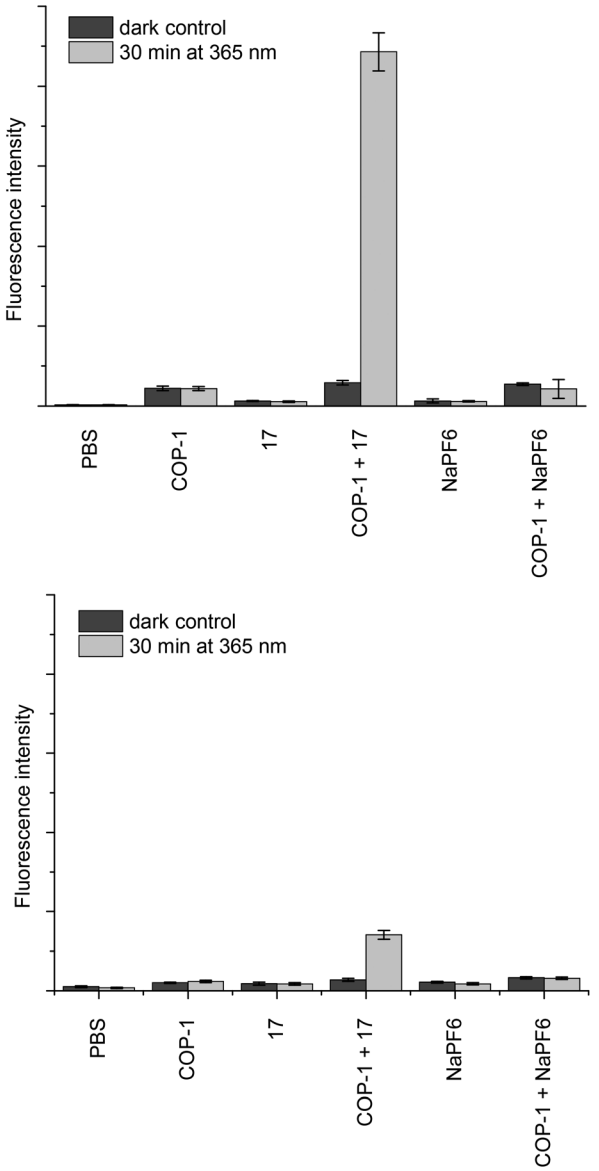

Fig. 12 Fluorescence intensity (λ_{ex} = 475 nm, λ_{em} = 510 nm) observed upon incubation of human umbilical vein endothelial cells (HUVECs) with **17** in (a) either the supernatant (top) and (b) the cell-containing fraction (bottom); black bars: dark control; grey bars: illuminated for 30 min at 365 nm, see the Experimental section for details; addition of (from left to right) PBS buffer only; COP-1 (10 μM) in PBS; **17** (100 μM) in PBS; COP-1 (10 μM) and **17** (100 μM) in PBS; $NaPF_6$ (100 μM) in PBS; COP-1 (10 μM) and $NaPF_6$ (100 μM) in PBS; the data are expressed as mean fluorescence intensity ± SD with experiments performed in quadruplicate. The fluorescence intensity is shown in arbitrary units at the same scale for both panels.

Conclusions

In the current report, a series of five manganese(I) tricarbonyl complexes based on the bis(2-pyrazolyl)ethylamine (bpea) moiety with a pendant *para*-substituted phenyl group in which R = H, I, or C≡C–H has been synthesized. The iodo and alkyne substituents will provide a flexible handle for bioconjugation *via* Sonogashira or CuAAC "click" reactions, for example, to further improve the bioavailability and targeting properties of these compounds, and the easy synthetic access to the bpea group will also allow facile preparation of additional derivatives with a tuned "drug sphere". All compounds are stable in DMSO solution and under the conditions of the myoglobin assay in the dark for a period of up to 14 h, thus establishing them as CORM prodrugs. However, they rapidly release about two equivalents of CO per mole of PhotoCORM upon illumination at 365 nm with half-lives in the range of 20–30 min, depending somewhat on the phenyl substituent and the imine *vs.* amine linker. Light-induced CO release could also be observed at 410 nm, although with a significantly longer half-life. MLCT transitions from the manganese to the pyrazole groups lead to a weakening of the metal–CO bond and the photolability of the carbonyl ligands, as inferred from DFT and TDDFT calculations. To demonstrate that this CO release also takes place under physiological conditions, the small-molecule fluorogenic switch-on carbon monoxide probe COP-1 was used to detect CO release from PhotoCORMs for the first time. While no response was observed in the presence of up to 10-fold excess of CORM over the probe when kept in the dark, illumination led to a rapid dose-dependent increase of the COP-1 fluorescence, which however did not show a linear relationship with the CORM concentration and did not fully saturate at even a 1 : 20 ratio of COP-1 to labile carbonyl ligands. When incubated with living HUVEC cells, COP-1 showed a significant response to light-induced CO release from one of the metal carbonyl complexes compared to dark controls as well as other additives. The effect was, however,

much more pronounced in the supernatant than in the cell-containing fraction (about 15-fold *vs.* 4-fold increase), indicating that the cellular uptake of either the CORM, the probe, or both will require further improvement although the system in general holds great promise as an *in vitro* reporter of carbon monoxide delivery from artificial carrier systems.

Experimental

General procedures

Reactions were carried out in oven-dried Schlenk glassware under an atmosphere of pure dinitrogen when necessary. Solvents were dried over molecular sieves and degassed prior to use. All reagents were purchased either from Sigma-Aldrich or Alfa Aesar and used without further purification. Manganese pentacarbonyl bromide was obtained from Strem Chemicals. 2,2′-Bis(pyrazol-1-yl)ethylamine (bpea) **5** was prepared according to the literature as described in the ESI.†[68,69] NMR spectra were recorded on Bruker DPX 200 and DRX 400 spectrometers (^{1}H: 200.13 and 400.13 MHz, respectively; ^{13}C: 50.33 and 100.62 MHz) at ambient temperature. Chemical shifts δ in ppm indicate a downfield shift relative to tetramethylsilane (TMS) and were referenced relative to the signal of the solvent.[70] Coupling constants J are given in Hz. Individual peaks are marked as singlet (s), doublet (d), doublet-of-doublet (dd), triplet (t), or multiplet (m). Mass spectra were measured on VG Autospec (FAB) and Bruker Esquire 6000 (ESI) instruments. 3-Nitrobenzylalcohol was used as the matrix in the FAB measurements. Data were recorded in positive ion mode. Infrared spectra were recorded for pure solid samples using a Bruker Tensor 27 IR spectrometer equipped with a Pike MIRacle Micro ATR accessory. The solution IR measurements were carried out with a Jasco FT/IR-4100 spectrometer using an IR flow-cell holder equipped with calcium fluoride windows (d = 4 mm) and a teflon spacer (d = 0.5 mm). The elemental analysis (C, H, N) of the compounds were performed with a VarioEL from Elementar Analysensysteme GmbH. The myoglobin assay and all photophysical studies were carried out in a quartz cuvette (d = 1 cm) with an Agilent 8453 UV/Vis diode array spectrophotometer using either a UV/Vis hand lamp (365 nm, UVIlite LF-206LS, 6 W, UVItec Ltd, Cambridge, UK) or a custom-built LED light source (407–412 nm wavelength range, 5 mm round type UV-LEDs, model YDG-504VC, Kingbright Elec. Co., Taipei, Taiwan, http://www.kingbright.com, part no. 181000-05).

Synthetic procedures

General procedure for the synthesis of bpea imine ligands 9–11. A solution of benzaldehyde (1.12 mL, 1.00 mmol for **9**), 4-iodobenzaldehyde (800 mg, 3.38 mmol for **10**), or 4-ethynylbenzaldehyde (365 mg, 2.83 mmol for **11**) in methanol (10 mL) was added dropwise to a stirred solution of 2,2′-bis(pyrazolyl)-ethylamine (2.00 g, 1.00 mmol for **9** or 600 mg, 3.38 mmol for **10** or 500 mg, 2.82 mmol for **11**) in methanol (60 mL) and heated to reflux overnight. The solvent was then removed under reduced pressure and the resulting solid was dried under vacuum.

9. Pale yellow solid, yield 73% (2.00 g, 0.01 mol). IR (ATR, ν/cm^{-1}): 3108 (w), 2852, 1649 (s, imine, C═N), 1514, 1434. ^{1}H NMR (200 MHz, $CDCl_3$, ppm): δ 8.20 (s, 1H, C**H**═N), 7.67 (d, 2H, ^3J = 2.4 Hz, $\mathbf{H}_{3,3'}$-pz), 7.56 (d, 2H, ^3J = 1.5 Hz, $\mathbf{H}_{5,5'}$-pz), 7.39 (m, 5H, $C_6\mathbf{H}_5$), 6.80 (t, 1H, ^3J = 7.00 Hz, C**H**(pz)$_2$), 6.25 (t, 2H, $\mathbf{H}_{4,4'}$-pz), 4.66 (d, 2H, ^3J = 6.8 Hz, C$\mathbf{H}_2$). ^{13}C-NMR (50.33 MHz, $CDCl_3$, ppm) δ 63.0 (**C**H$_2$), 75.2 (**C**(pz)$_2$), 106.6 ($\mathbf{C}_4$-pz), 128.4 ($\mathbf{C}_{3,5}$–C_6H_5), 128.7 ($\mathbf{C}_{2,6}$–C_6H_5), 129.2 ($\mathbf{C}_4$–C_6H_5), 131.3 ($\mathbf{C}_5$-pz), 135.8 ($\mathbf{C}_1$–C_6H_5), 140.5 ($\mathbf{C}_3$-Pz), 164.9 (**C**═N). MS (FAB+): m/z 266 [M + H]$^+$. Elemental analysis (%): calc. for $C_{15}H_{15}N_5$: C 67.90, H 5.69, N 26.39; found: C 67.75, H 5.88, N 26.74.

10. White solid, yield 88% (1.17 g, 2.99 mmol). IR (ATR, ν/cm^{-1}): 3100 (w), 1644 (s, imine, C═N), 1586, 1510, 1436, 1387. ^{1}H NMR (200 MHz, $CDCl_3$, ppm): δ 8.11 (s, 1H, C**H**═N), 7.71 (d, 2H, ^3J = 8.4 Hz, $\mathbf{H}_{3,5}$–C_6H_4), 7.65 (d, 2H, ^3J = 2.3 Hz, $\mathbf{H}_{3,3'}$-pz), 7.55 (d, 2H, ^3J = 1.5 Hz, $\mathbf{H}_{5,5'}$-pz), 7.34 (d, 2H, ^3J = 8.4 Hz, $\mathbf{H}_{2,6}$–C_6H_4), 6.77 (t, 1H, ^3J = 6.8 Hz, C**H**(pz)$_2$), 6.25 (t, 2H, $\mathbf{H}_{4,4'}$-pz), 4.64 (d, 2H, ^3J = 6.8 Hz, C$\mathbf{H}_2$). ^{13}C-NMR (100.62 MHz, $CDCl_3$, ppm) δ 63.0 (**C**H$_2$), 75.1 (**C**(pz)$_2$), 98.1 ($\mathbf{C}_4$–C_6H_4), 106.6 ($\mathbf{C}_4$-pz), 129.2 ($\mathbf{C}_5$-pz), 129.8 ($\mathbf{C}_{2,6}$–C_6H_4), 135.2 ($\mathbf{C}_1$–C_6H_4), 138.0 ($\mathbf{C}_{3,5}$–C_6H_4), 140.5 ($\mathbf{C}_3$-pz), 163.9 (**C**═N). MS (FAB+): m/z 392 [M + H]$^+$, 414 [M + Na]$^+$. Elemental analysis (%): calc. for $C_{15}H_{14}N_5I$: C 46.05, H 3.60, N 17.90; found: C 46.14, H 3.69, N 17.82.

11. Colorless solid, yield 72% (585 mg, 2.02 mmol). IR (ATR, ν/cm^{-1}): 3254 (w), 3137, 2917, 2105 (C≡C), 1641 (s, imine, C═N), 1556, 1433. ^{1}H NMR (400 MHz, $CDCl_3$, ppm): δ 8.17 (s, C**H**═N), 7.66 (d, 2H, ^3J = 2.4 Hz, $\mathbf{H}_{3,3'}$-pz), 7.57 (d, 2H, ^3J = 8.4 Hz, $\mathbf{H}_{3,5}$–C_6H_4), 7.55 (d, 2H, ^3J = 1.6 Hz, $\mathbf{H}_{5,5'}$-pz), 7.47 (d, 2H, ^3J = 8.4 Hz, $\mathbf{H}_{2,6}$–C_6H_4), 6.78 (t, 1H, ^3J = 6.8 Hz, C**H**(pz)$_2$), 6.25 (t, 2H, $\mathbf{H}_{4,4'}$-pz), 4.67 (d, 2H, ^3J = 6.8 Hz, C$\mathbf{H}_2$), 3.16 (s, 1H, C≡C–**H**). ^{13}C-NMR (100.62 MHz, $CDCl_3$, ppm) δ 63.0 (**C**H$_2$), 75.2 (C≡**C**H), 79.3 (**C**(pz)$_2$), 83.3 (**C**≡CH), 106.6 ($\mathbf{C}_4$-pz), 125.0 ($\mathbf{C}_4$–C_6H_4), 128.2 ($\mathbf{C}_{2,6}$–C_6H_4), 129.2 ($\mathbf{C}_5$-pz), 132.4 ($\mathbf{C}_{3,5}$–C_6H_4), 135.9 ($\mathbf{C}_1$–C_6H_4), 140.5 ($\mathbf{C}_3$-pz), 164.0 (**C**═N). MS (FAB+): m/z 290 [M + H]$^+$, 312 [M + Na]$^+$. Elemental analysis (%): calc. for $C_{17}H_{15}N_5$: C 70.57, H 5.22, N 24.20; found: C 70.49, H 5.31, N 24.27.

General procedure for the synthesis of bpea amine ligands 12–13. An excess of solid sodium borohydride (65 mg, 1.72 mmol for **12** or 38 mg, 1.02 mmol for **13**) was added in portions to a solution of **9** (230 mg, 0.86 mmol) or **10** (160 mg, 0.41 mmol) in methanol (10 mL) and then stirred for 6 h at room temperature. Water (5 mL) was added to the reaction mixture. The solvent was then removed under vacuum and the residue was redissolved in ethyl acetate (40 mL) and washed with water (3 × 50 mL). The organic phase was separated, dried over sodium sulfate (~5 g), and filtered. The solvent was then removed from the filtrate under reduced pressure and the resulting solid was dried *in vacuo*.

12. Pale yellow solid, yield 78% (178 mg, 0.66 mmol). IR (ATR, ν/cm^{-1}): 3341 (m, NH), 3137, 2830, 1599, 1493, 1367. ^{1}H-NMR (400 MHz, $CDCl_3$, ppm): δ 7.58 (d, 2H, ^3J = 2.4 Hz, $\mathbf{H}_{3,3'}$-pz), 7.55 (d, 2H, ^3J = 1.7 Hz, $\mathbf{H}_{5,5'}$-pz), 7.28 (m, 5H, $C_6\mathbf{H}_5$),

6.54 (t, 1H, ^3J = 7 Hz, C**H**(pz)$_2$), 6.27 (m, 2H, **H**$_{4,4'}$-pz), 3.83 (s, 2H, C**H**$_2$–C$_6$H$_5$), 3.70 (d, 2H, ^3J = 7.0 Hz, C**H**$_2$). ^{13}C-NMR (100.62 MHz, $CDCl_3$, ppm) δ 51.2 (**C**H$_2$), 53.4 (**C**H$_2$–C$_6$H$_5$), 75.2 (**C**(pz)$_2$), 106.8 (**C**$_4$-pz), 127.3 (**C**$_4$–C$_6$H$_5$), 128.2 (**C**$_{3,5}$–C$_6$H$_5$), 128.7 (**C**$_{2,6}$–C$_6$H$_5$), 129.1 (**C**$_5$-pz), 139.8 (**C**$_1$–C$_6$H$_5$), 140.4 (**C**$_3$-pz). MS (FAB+): m/z 268 [M + H]$^+$, 290 [M + Na]$^+$. Elemental analysis (%): calc. for $C_{15}H_{17}N_5$: C 67.39, H 6.40, N 26.19; found: C 67.12, H 6.35, N 26.61.

13. Colorless solid, yield 72% (115 mg, 0.29 mmol). IR (ATR, ν/cm^{-1}): 3327 (m, NH), 3090, 2928, 1510, 1482, 1387, 1283. ^{1}H-NMR (400 MHz, $CDCl_3$, ppm): δ 7.62 (d, 2H, ^3J = 8.3 Hz, **H**$_{3,5}$–C$_6$H$_4$), 7.57 (d, 2H, ^3J = 2.4 Hz, **H**$_{3,3'}$-pz), 7.55 (d, 2H, ^3J = 1.5 Hz, **H**$_{5,5'}$-pz), 7.02 (d, 2H, ^3J = 8.3 Hz, **H**$_{2,6}$–C$_6$H$_4$), 6.52 (t, 1H, ^3J = 7 Hz, C**H**(pz)$_2$), 6.27 (t, 2H, **H**$_{4,4'}$-pz), 3.76 (s, 2H, C**H**$_2$–C$_6$H$_4$), 3.66 (d, 2H, ^3J = 6.9 Hz, C**H**$_2$). ^{13}C-NMR (100.62 MHz, $CDCl_3$, ppm) δ 51.1 (**C**H$_2$), 52.8 (**C**H$_2$–C$_6$H$_4$), 75.2 (**C**(pz)$_2$), 92.6 (**C**$_4$–C$_6$H$_4$), 106.9 (**C**$_4$-pz), 129.1 (**C**$_{3,5}$–C$_6$H$_4$), 120.1 (**C**$_{2,6}$–C$_6$H$_4$), 137.7 (**C**$_5$-pz), 139.6 (**C**$_1$–C$_6$H$_4$), 140.5 (**C**$_3$-pz). MS (FAB+): m/z 394 [M + H]$^+$, 416 [M + Na]$^+$. Elemental analysis (%): calc. for $C_{15}H_{16}N_5I$: C 45.81, H 4.10, N 17.80; found: C 45.66, H 4.23, N 17.69.

General procedure for the synthesis of manganese(I) tricarbonyl-bpea complexes (14–18). To a stirred solution of manganese pentacarbonyl bromide (206 mg, 0.75 mmol) in anhydrous acetone (45 mL) was added a solution of **9** (200 mg, 0.75 mmol for **14**), **10** (293 mg, 0.75 mmol for **15**), **11** (217 mg, 0.75 mmol for **16**), **12** (200 mg, 0.75 mmol for **17**), or **13** (295 mg, 0.75 mmol for **18**) in anhydrous acetone (5 mL) and the mixture was heated to reflux for 5 h under a dinitrogen atmosphere with exclusion of light. The solvent was then removed under vacuum. The yellow residue was washed with diethylether, redissolved in methanol (10 mL) and an aqueous solution of potassium hexafluorophosphate (1.2 equiv.) was added. The precipitated product was filtered off, washed with water and diethylether, and dried under vacuum.

*[Mn(CO)$_3$(bpea$^{N=CHC6H5}$)]PF$_6$ (**14**).* Yellow solid, yield 64% (263 mg, 0.48 mmol). IR (ATR, ν/cm^{-1}): 3135 (w), 2962 (w), 2040 (s, C≡O), 1932 (s, C≡O), 1625 (s, imine, C=N), 1414, 1261, 1102, 1065. ^{1}H-NMR (400 MHz, acetone-d_6, ppm): δ 9.41 (s, 1H, C**H**=N), 8.45 (d, 2H, ^3J = 2.7 Hz, **H**$_{5,5'}$-pz), 8.38 (d, 2H, ^3J = 2.3 Hz, **H**$_{3,3'}$-pz), 7.81 (t, 1H, ^3J = 2.5 Hz, C**H**(pz)$_2$), 7.66 (m, 5H, C$_6$**H**$_5$), 6.75 (t, 2H, ^3J = 2.5 Hz, **H**$_{4,4'}$-pz), 4.67 (dd, 2H, ^3J = 2.6 Hz, 2.1 Hz, C**H**$_2$). ^{13}C-NMR (100.62 MHz, acetone-d_6, ppm) δ 63.0 (**C**H$_2$), 69.7 (**C**(pz)$_2$), 109.6 (**C**$_4$-pz), 129.0 (**C**$_4$–C$_6$H$_5$), 129.7 (**C**$_{3,5}$–C$_6$H$_5$), 132.3 (**C**$_{2,6}$–C$_6$H$_5$), 135.8 (**C**$_5$-pz), 136.9 (**C**$_1$–C$_6$H$_5$), 146.8 (**C**$_3$-pz), 181.6 (**C**=N). MS (ESI$^+$, MeOH): m/z 403.82 [M − PF$_6$]$^+$. Elemental analysis (%): calc. for $C_{18}H_{15}F_6MnN_5O_3P{\cdot}H_2O$: C 38.11, H 3.02, N 12.35; found: C 38.36, H 2.83, N 11.99.

*[Mn(CO)$_3$(bpea$^{N=CHC6H4I}$)]PF$_6$ (**15**).* Yellow solid, yield 43% (216 mg, 0.32 mmol). IR (ATR, ν/cm^{-1}): 3135 (w), 3021 (w), 2043 (s, C≡O), 1931 (s, C≡O), 1624 (s, imine, C=N), 1412, 1295, 1103. ^{1}H-NMR (400 MHz, acetone-d_6, ppm): δ 9.34 (s, 1H, C**H**=N), 8.43 (d, 2H, ^3J = 2.7 Hz, **H**$_{5,5'}$-pz), 8.38 (d, 2H, ^3J = 2.2 Hz, **H**$_{3,3'}$-pz), 8.03 (d, 2H, ^3J = 4.7 Hz, **H**$_{3,5}$–C$_6$H$_4$), 7.76 (t, 1H, ^3J = 2.7 Hz, C**H**(pz)$_2$), 7.52 (d, 2H, ^3J = 8.1 Hz, **H**$_{2,6}$–C$_6$H$_4$), 6.75 (t, 2H, **H**$_{4,4'}$-pz), 4.63 (d, 2H, C**H**$_2$). ^{13}C-NMR (100.62 MHz, acetone-d_6, ppm) δ 51.4 (**C**H$_2$), 58.0 (**C**(pz)$_2$), 88.7 (**C**$_4$–C$_6$H$_4$), 98.8 (**C**$_4$-pz), 120.0, 123.0, 125.2, 127.8, 128.0, 137.0 (**C**$_3$-pz), 164.9, 171.1 (**C**=N). MS (ESI$^+$, CH$_3$OH): m/z 529.81 [M − PF$_6$]$^+$. Elemental analysis (%): calc. for $C_{18}H_{14}F_6IMnN_5O_3P$: C 32.02, H 2.09, N 10.37; found: C 31.83, H 1.91, N 10.26.

*[Mn(CO)$_3$(bpea$^{N=CHC6H4C\equiv CH}$)]PF$_6$ (**16**).* Yellow solid, yield: 82% (355 mg, 0.62 mmol). IR (ATR, ν/cm^{-1}): 3277 (m, N–H), 3138 (w), 3021 (w), 2041 (s, C≡O), 1930 (s, C≡O), 1633 (s, imine, C=N), 1458, 1365, 1262, 1019. ^{1}H-NMR (400 MHz, acetone-d_6, ppm): δ 9.39 (s, 1H, C**H**=N), 8.43 (d, 2H, ^3J = 2.7 Hz, **H**$_{5,5'}$-pz), 8.37 (d, 2H, ^3J = 2.2 Hz, **H**$_{3,3'}$-pz), 7.73 (m, 5H, C**H**(pz)$_2$, C$_6$**H**$_4$), 6.74 (t, 2H, **H**$_{4,4'}$-pz), 4.63 (d, 2H, C**H**$_2$), 3.88 (s, 1H, C≡C–**H**). ^{13}C-NMR (100.62 MHz, acetone-d_6, ppm) δ 62.9 (**C**H$_2$), 69.6 (C≡**C**H), 81.7 (**C**(pz)$_2$), 83.3 (**C**≡CH), 109.6 (**C**$_4$-pz), 126.2 (**C**$_4$–C$_6$H$_4$), 129.3 (**C**$_{2,6}$–C$_6$H$_4$), 133.1 (**C**$_{3,5}$–C$_6$H$_4$), 135.7 (**C**$_5$-pz), 137.0 (**C**$_1$–C$_6$H$_4$), 147.8 (**C**$_3$-pz), 181.9 (**C**=N), 220.3 (C≡O). MS (ESI$^+$, CH$_3$OH): m/z 427.84 [M − PF$_6$]$^+$. Elemental analysis (%): calc. for $C_{20}H_{15}F_6MnN_5O_3P$: C 41.90, H 2.64, N 12.22; found: C 41.98, H 2.54, N 12.28.

*[Mn(CO)$_3$(bpea^{NHCH2C6H5})]PF$_6$ (**17**).* Yellow solid, yield: 69% (283 mg, 0.51 mmol). IR (ATR, ν/cm^{-1}): 3307 (m, N–H), 2045 (s, C≡O), 1939 (s, C≡O), 1604, 1519, 1450, 1315. ^{1}H-NMR (400 MHz, acetone-d_6, ppm): δ 8.51 (d, 1H, ^3J = 2.3 Hz, **H**$_{3'}$-pz), 8.39 (d, 1H, ^3J = 2.3 Hz, **H**$_3$-pz), 8.33 (d, 1H, ^3J = 2.7 Hz, **H**$_{5'}$-pz), 8.27 (d, 1H, ^3J = 2.7 Hz, **H**$_5$-pz), 7.41 (m, 6H, C**H**(pz)$_2$, C$_6$**H**$_5$), 6.74 (t, 1H, ^3J = 2.5 Hz, **H**$_4$-pz), 6.66 (t, 1H, ^3J = 2.5 Hz, **H**$_{4'}$-pz), 5.59 (s, br, 1H, N**H**), 4.69 (dd, 1H, ^3J = 13.4, 4.1 Hz, H$_b$–C**H**$_2$–C$_6$H$_5$), 4.20 (dd, 1H, ^3J = 13.4, 10.1 Hz, H$_b$–C**H**$_2$–C$_6$H$_5$), 3.52 (ddd, 1H, ^3J = 13.9, 7.8, 4.0 Hz, H$_{a'}$–C**H**$_2$), 3.12 (ddd, 1H, ^3J = 13.9, 8.9, 1.4 Hz, H$_a$–C**H**$_2$). ^{13}C-NMR (100.62 MHz, acetone-d_6, ppm) δ 50.3 (**C**H$_2$–N), 62.3 (**C**H$_2$–C$_6$H$_5$), 68.7 (**C**(pz)$_2$), 108.3 (**C**$_4$-pz), 108.4 (**C**$_{4'}$-pz), 128.5, 128.7, 129.6, 134.3 (**C**$_5$-pz), 134.7 (**C**$_{5'}$-pz), 135.8 (**C**$_1$–C$_6$H$_5$), 147.0 (**C**$_3$-pz), 147.1 (**C**$_{3'}$-pz). MS (ESI$^+$, CH$_3$OH): m/z 405.92 [M − PF$_6$]$^+$. Elemental analysis (%): calc. for $C_{18}H_{17}F_6MnN_5O_3P$: C 39.22, H 3.11, N 12.70; found: C 39.21, H 3.27, N 12.76.

*[Mn(CO)$_3$(bpea^{NHCH2C6H4I})]PF$_6$ (**18**).* Yellow solid, yield: 43% (218 mg, 0.32 mmol). IR (ATR, ν/cm^{-1}): 3275 (m, N–H), 3139 (w), 2962 (w), 2041 (s, C≡O), 1928 (s, C≡O), 1520, 1443, 1307, 1261, 1148, 1065. ^{1}H-NMR (400 MHz, acetone-d_6, ppm): δ 8.51 (d, 1H, ^3J = 2.2 Hz, **H**$_{3'}$-pz), 8.40 (d, 1H, ^3J = 2.2 Hz, **H**$_3$-pz), 8.32 (d, 1H, ^3J = 2.3 Hz, **H**$_{5'}$-pz), 8.27 (d, 1H, ^3J = 2.4 Hz, **H**$_5$-pz), 7.76 (d, 2H, ^3J = 8.4 Hz, **H**$_{2,6}$–C$_6$H$_4$), 7.43 (d, 1H, ^3J = 3.1 Hz, C**H**(pz)$_2$), 7.30 (d, 2H, ^3J = 8.3 Hz, **H**$_{3,5}$–C$_6$H$_4$), 6.74 (t, 1H, ^3J = 2.5 Hz, **H**$_{4'}$-pz), 6.67 (t, 1H, ^3J = 2.5 Hz, **H**$_4$-pz), 5.60 (s, 1H, N**H**), 4.68 (dd, 1H, ^3J = 13.5, ^2J = 4.0 Hz, H$_{b'}$–C**H**$_2$–C$_6$H$_4$), 4.21 (dd, 1H, ^3J = 13.5, ^3J = 10.2 Hz, H$_b$–C**H**$_2$–C$_6$H$_4$), 3.55 (ddd, 1H, ^3J = 13.7, ^3J = 7.8, ^2J = 3.8 Hz, H$_{a'}$–C**H**$_2$), 3.12 (dd, 1H, ^3J = 13.7, ^3J = 8.9 Hz, H$_a$–C**H**$_2$). ^{13}C-NMR (100.62 MHz, acetone-d_6, ppm) δ 51.2 (**C**H$_2$), 62.4 (**C**H$_2$–C$_6$H$_4$), 69.6 (**C**(pz)$_2$), 94.8 (**C**$_4$–C$_6$H$_4$), 109.3 (**C**$_4$-pz), 132.7 (**C**$_3$–C$_6$H$_4$), 135.2 (**C**$_5$-pz), 135.7 (**C**$_{5'}$-pz), 136.6 (**C**$_1$–C$_6$H$_4$), 138.7 (**C**$_{2,6}$–C$_6$H$_4$), 148.0 (**C**$_3$-pz), 148.1 (**C**$_{3'}$-pz). MS (ESI$^+$, CH$_3$OH): m/z 531.77 [M − PF$_6$]$^+$. Elemental analysis (%): calc. for $C_{18}H_{17}F_6MnN_5O_3P$: C 31.93, H 2.38, N 10.34; found: C 32.01, H 2.31, N 10.46.

Myoglobin assay

In a quartz cuvette, a solution of horse skeletal muscle myoglobin in 0.1 M phosphate buffer (PBS, pH 7.4) was degassed by bubbling with dinitrogen and reduced by addition of sodium dithionite (100 mM, 100 μL) in PBS buffer (0.1 M, pH 7.4) to a total volume of 614 μL. To this solution, 10 μL of **14–18** in dimethylsulfoxide was added followed by PBS to give a total volume of 1000 μL with final concentrations of 10 μM of CORM, 10 mM of sodium dithionite, 60 μM of myoglobin with $A_{557} < 1$. The solutions were freshly prepared for both the dark stability measurements and the photoactivation experiments. Illumination was carried out under dinitrogen either using a UV/Vis hand lamp (365 nm, UVIlite LF-206LS, 6 W, UVItec Ltd, Cambridge, UK) or a custom-built LED light source (407–412 nm wavelength range, 5 mm round type UV-LEDs, model YDG-504VC, Kingbright Elec. Co., Taipei, Taiwan, http://www.kingbright.com, part no. 181000-05), both positioned perpendicular to the cuvette at a distance of 3 cm. The illumination was interrupted in regular intervals to record UV/Vis spectra on an Agilent 8453 UV/Vis diode array spectrophotometer. As a dark control, measurements were carried out by using the automated spectrometer software for a predefined period of time (14 h). All experiments were carried out in triplicate.

Photolysis experiments monitored by solution IR spectroscopy

An IR flow-cell holder equipped with calcium fluoride windows and a Teflon spacer was filled with a freshly prepared solution of 14 or 17 in DMSO (9 mM). Illuminations were then carried out using an UV/Vis hand lamp (365 nm, UVIlite LF-206LS, 6 W, UVItec Ltd, Cambridge, UK) with the flow-cell positioned at a distance of 3 cm. The illumination was interrupted in regular intervals and IR spectra recorded on a Jasco FT/IR-4100 spectrometer.

Ferrioxalate actinometry

Ferrioxalate actinometry was used to determine the photon flux of the 365 nm UV hand lamp because of its sensitivity, wide spectral range including the ultraviolet, and the ease of use.[71,72] The whole ferrioxalate actinometry procedure including the preparation of solutions was carried out under red safe-light. The concentration of ferrous iron formed was determined spectrophotometrically by complexation with 1,10-phenanthroline (phen) to give the colored tris-phenanthroline complex $[Fe(phen)_3]^{2+}$ at λ_{max} = 510 nm. Thus, in a 1 cm quartz cell, potassium ferrioxalate (0.006 M) in sulfuric acid (0.05 M, 3 mL) as the chemical actinometer was illuminated with a 365 nm UV hand lamp (6 W, UVITEC, UK) positioned 3 cm from the cuvette under efficient stirring. The illuminated solution (1 mL) was mixed with 0.1% 1,10-phenanthroline in water (1 mL) and aqueous sodium acetate buffer (0.5 mL, 1 M, pH 3.5), and then further diluted to 10 mL with water. A reference sample was prepared in the same way but without the illumination. Both solutions were placed in the dark (about 1 h) to allow the complexation to complete. The absorbance was then measured at 510 nm (ε = 11 100 M^{-1} cm^{-1}). A_{510} was kept within the range of 0.4–1.0. The photon flux of the 365 nm UV hand lamp was then calculated using $\Phi_{365\ nm}$ = 1.21 following the equation:[73]

$$\Phi_p = \frac{\Delta A V_1 10^{-3} V_3}{\Phi_\lambda \varepsilon_{510} V_2 t}$$

Cells and cell culture conditions

Human umbilical vein endothelial cells (HUVECs) were received in collaboration with the Institute of Transfusion Medicine and Immunology, Medical Faculty Mannheim, University of Heidelberg. Permission for isolation and propagation of endothelial cells from umbilical cords for research purposes was granted by the local ethics committee of the clinical faculty Mannheim, University of Heidelberg with informed consent in writing. HUVECs were isolated from fresh umbilical cords as described previously.[74] The cells were cultured in endothelial cell growth medium (EGM) (Promocell, Heidelberg, Germany) in T25 flasks (Greiner, Frickenhausen, Germany) coated with gelatin (1%). Confluent monolayers were passaged by trypsin/EDTA (Sigma-Aldrich, St. Louis, MO). Characterization of endothelial cells was performed on the basis of a positive uptake of acetylated LDL, Factor VIII related antigen, and PECAM (CD31) expression, and a negative staining for alpha smooth muscle actin.

In vitro detection of CO release using the COP-1 fluorogenic switch-on probe

(a) In phosphate-buffered saline. On a 96-well microtiter plate, phosphate-buffered saline (PBS, 100 μL) containing different final concentrations of compound **17** (3–100 μM) dissolved in DMSO was added to each well and then, COP-1 dissolved in PBS was added to a final concentration of 10 μM. The plate was subsequently exposed for 30 min to UV light at 365 nm from a 6 W lamp (UVITEC Cambridge, UK) positioned parallel to the plate at a distance of 3 cm. Meanwhile, another plate was prepared under the same experimental conditions but kept in the dark for 30 min. The fluorescence was measured immediately afterwards on an Infinite M200 reader (Tecan, Crailsheim, Germany) using the I-control v9 software. The fluorescence intensity was assessed at excitation and emission wavelengths of 475 and 510 nm, respectively. The experiments along with the controls were performed in quadruplicate and the data are expressed as mean fluorescence intensity ± SD.

(b) In cell culture. HUVECs were seeded in 96-well plates (Greiner, Frickenhausen, Germany) at a concentration of 10^5 cells per well. After 1 d of seeding, the supernatant was aspirated and replaced by a freshly prepared solution of compound **17** in DMSO diluted with PBS to a final concentration of 100 μM and COP-1 dissolved in PBS was added to a final concentration of 10 μM. As negative controls, pure PBS buffer, COP-1 (10 μM), **17** (100 μM) and sodium hexafluorophosphate (100 μM) were also included in the experiments. One plate was subsequently exposed for 30 min to UV light at 365 nm from a

6 W lamp (LF-206-LS, UVITEC, Cambridge, UK) positioned parallel to the plate at a distance of 3 cm. Meanwhile, another plate was prepared under the same experimental conditions but kept in the dark for 30 min. After exposure, the whole supernatant was transferred to a fresh plate to measure the fluorescence intensity in the fluid phase. The cell-containing plates were washed with PBS (2×) and after the last wash, 100 μL of PBS was added to each well. The fluorescence intensity associated with the fluid phase and the cells was measured separately on an Infinite M200 reader (Tecan, Crailsheim, Germany) using the I-control v9 software. The fluorescence intensity was assessed at an excitation and emission wavelength of 475 and 510 nm, respectively. The experiments along with the controls were performed in quadruplicate and the data are expressed as mean fluorescence intensity ± SD.

Density functional theory calculations

DFT calculations were carried out on the Linux cluster of the Leibniz-Rechenzentrum (LRZ) in Munich with ORCA version 2.8,[75] using the BP86 functional with the resolution-of-the-identity (RI) approximation, a def2-TZVP/def2-TZVP/J basis set,[76,77] the tightscf and grid4 options, and the COSMO solvation model with dimethylsulfoxide as the solvent for geometry optimizations and subsequent calculation of vibrational frequencies to characterize the structures obtained as minima by inspection for the absence of imaginary modes. Reported vibrational modes are scaled with a factor of 1.036 relative to the calculated values. The TDDFT calculations employed the B3LYP functional with the same basis set and settings as above using the RIJCOSX keyword. The first 45 singlet excited states were calculated (nroots 45).

X-ray crystallography

A single crystal of **15**, **17**, or **18** was immersed in a film of perfluoropolyether oil, mounted on a glass fiber and transferred to a stream of cold nitrogen of the diffractometer. Diffraction data were collected on an Oxford Diffraction system using a Sapphire2-CCD detector for **17** and a Multiwire Proportional counter for **15** and **18** at 110–113 K and using graphite monochromated Mo-Kα radiation (λ = 0.71073 Å). The final cell constants were obtained from a least squares fit of a subset of a few thousand strong reflections. The program CrysAlis CCD was used for data collection. CrysAlis RED and CrysAlis CCD software were used for cell refinements and data reduction. The program SADABS was used to account for the absorption.[78] The OLEX 2 program was used for refinement and artwork of the structure.[79] Crystallographic data (excluding structure factors) have been deposited with the Cambridge Crystallographic Data Centre as supplementary publications No. CCDC 976263, 976264, and 976267.

Acknowledgements

This work was supported by the Deutsche Forschungsgemeinschaft (DFG) within the project FOR 630 "Biological function of organometallic compounds". The stay of G.A. in Germany was supported by the DAAD with an IAESTE fellowship. We would like to thank Manuela Winter and Timo Bollermann for help with some of the X-ray structure analysis.

References

1 L. Wu and R. Wang, *Pharmacol. Rev.*, 2005, **57**, 585–630.
2 H. P. Kim, S. W. Ryter and A. M. K. Choi, *Annu. Rev. Pharmacol. Toxicol.*, 2006, **46**, 411–449.
3 M. Kajimura, R. Fukuda, R. M. Bateman, T. Yamamoto and M. Suematsu, *Antioxid. Redox Signaling*, 2010, **13**, 157–192.
4 L. Rochette, Y. Cottin, M. Zeller and C. Vergely, *Pharmacol. Ther.*, 2013, **137**, 133–152.
5 S. W. Ryter, J. Alam and A. M. K. Choi, *Physiol. Rev.*, 2006, **86**, 583–650.
6 N. G. Abraham and A. Kappas, *Pharmacol. Rev.*, 2008, **60**, 79–127.
7 T. Matsui, M. Iwasaki, R. Sugiyama, M. Unno and M. Ikeda-Saito, *Inorg. Chem.*, 2010, **49**, 3602–3609.
8 T. Matsui, M. Unno and M. Ikeda-Saito, *Acc. Chem. Res.*, 2010, **43**, 240–247.
9 R. Motterlini and L. E. Otterbein, *Nat. Rev. Drug Discovery*, 2010, **9**, 728–743.
10 B. Wegiel, D. W. Hanto and L. E. Otterbein, *Trends Mol. Med.*, 2013, **19**, 3–11.
11 L. S. Nobre, J. D. Seixas, C. C. Romao and L. M. Saraiva, *Antimicrob. Agents Chemother.*, 2007, **51**, 4303–4307.
12 J. L. Wilson, H. E. Jesse, R. K. Poole and K. S. Davidge, *Curr. Pharm. Des.*, 2012, **13**, 760–768.
13 C. C. Romao, W. A. Blättler, J. D. Seixas and G. J. L. Bernardes, *Chem. Soc. Rev.*, 2012, **41**, 3571–3583.
14 B. E. Mann, in *Top. Organomet. Chem.*, ed. N. Metzler-Nolte and G. Jaouen, Springer, Berlin, 2010, vol. 32, pp. 247–285.
15 B. E. Mann, *Organometallics*, 2012, **31**, 5728–5735.
16 F. Zobi, *Future Med. Chem.*, 2013, **5**, 175–188.
17 U. Schatzschneider, *Br. J. Pharmacol.*, 2014, DOI: 10.1111/bph.12688.
18 R. Motterlini, P. Sawle, S. Bains, J. Hammad, R. Alberto, R. Foresti and C. J. Green, *FASEB J.*, 2004, **18**, 284–286.
19 T. S. Pitchumony, B. Spingler, R. Motterlini and R. Alberto, *Chimia*, 2008, **62**, 277–279.
20 T. S. Pitchumony, B. Spingler, R. Motterlini and R. Alberto, *Org. Biomol. Chem.*, 2010, **8**, 4849–4954.
21 L. A. P. Antony, T. Slanina, P. Sebej, T. Solomek and P. Klan, *Org. Lett.*, 2013, **15**, 4552–4555.
22 P. Peng, C. Wang, Z. Shi, V. K. Johns, Y. Ma, J. Oyer, A. Copik, R. Igarashi and Y. Liao, *Org. Biomol. Chem.*, 2013, **11**, 6671–6674.
23 T. R. Johnson, B. E. Mann, I. P. Teasdale, H. Adams, R. Foresti, C. J. Green and R. Motterlini, *Dalton Trans.*, 2007, 1500–1508.
24 S. Romanski, B. Kraus, U. Schatzschneider, J. Neudörfl, S. Amslinger and H.-G. Schmalz, *Angew. Chem., Int. Ed.*, 2011, **50**, 2392–2396.

25 S. Romanski, B. Kraus, M. Guttentag, W. Schlundt, H. Rücker, A. Adler, J.-M. Neudörfl, R. Alberto, S. Amslinger and H.-G. Schmalz, *Dalton Trans.*, 2012, **41**, 13862–13875.
26 S. Romanski, H. Rücker, E. Stamellou, M. Guttentag, J. Neudörfl, R. Alberto, S. Amslinger, B. Yard and H.-G. Schmalz, *Organometallics*, 2012, **31**, 5800–5809.
27 S. Botov, E. Stamellou, S. Romanski, M. Guttentag, R. Alberto, J. Neudörfl, B. Yard and H.-G. Schmalz, *Organometallics*, 2013, **32**, 3587–3594.
28 P. C. Kunz, H. Meyer, J. Barthel, S. Sollazzo, A. M. Schmidt and C. Janiak, *Chem. Commun.*, 2013, **49**, 4896–4898.
29 U. Schatzschneider, *Eur. J. Inorg. Chem.*, 2010, 1451–1467.
30 U. Schatzschneider, *Inorg. Chim. Acta*, 2011, **374**, 19–23.
31 R. D. Rimmer, A. E. Pierri and P. C. Ford, *Coord. Chem. Rev.*, 2012, **256**, 1509–1519.
32 V. P. Lorett-Velasquez, T. M. A. Jazzazi, A. Malassa, H. Görls, G. Gessner, S. H. Heinemann and M. Westerhausen, *Eur. J. Inorg. Chem.*, 2012, 1072–1078.
33 R. Kretschmer, G. Gessner, H. Görls, S. H. Heinemann and M. Westerhausen, *J. Inorg. Biochem.*, 2011, **105**, 6–9.
34 M. A. Gonzalez, N. L. Fry, R. Burt, R. Davda, A. Hobbs and P. K. Mascharak, *Inorg. Chem.*, 2011, **50**, 3127–3134.
35 C. S. Jackson, S. Schmitt, Q. P. Dou and J. J. Kodanko, *Inorg. Chem.*, 2011, **50**, 5336–5338.
36 H. Pfeiffer, T. Sowik and U. Schatzschneider, *J. Organomet. Chem.*, 2013, **734**, 17–24.
37 R. D. Rimmer, H. Richter and P. C. Ford, *Inorg. Chem.*, 2010, **49**, 1180–1185.
38 A. E. Pierri, A. Pallaoro, G. Wu and P. C. Ford, *J. Am. Chem. Soc.*, 2012, **134**, 18197–18200.
39 J. S. Ward, J. M. Lynam, J. W. B. Moir, D. E. Sanin, A. P. Mountford and I. J. S. Fairlamb, *Dalton Trans.*, 2012, **41**, 10514–10517.
40 M. A. Gonzalez, M. A. Yim, S. Cheng, A. Moyes, A. J. Hobbs and P. K. Mascharak, *Inorg. Chem.*, 2012, **51**, 601–608.
41 M. A. Gonzalez, S. J. Carrington, N. L. Fry, J. L. Martinez and P. K. Mascharak, *Inorg. Chem.*, 2012, **51**, 11930–11940.
42 S. J. Carrington, I. Chakraborty and P. K. Mascharak, *Chem. Commun.*, 2013, **49**, 11254–11256.
43 M. A. Gonzalez, S. J. Carrington, I. Chakraborty, M. M. Olmstead and P. K. Mascharak, *Inorg. Chem.*, 2013, **52**, 11320–11331.
44 W. Huber, R. Linder, J. Niesel, U. Schatzschneider, B. Spingler and P. C. Kunz, *Eur. J. Inorg. Chem.*, 2012, 3140–3146.
45 F. Mohr, J. Niesel, U. Schatzschneider and C. W. Lehmann, *Z. Anorg. Allg. Chem.*, 2012, **638**, 543–546.
46 J. Niesel, A. Pinto, H. W. Peindy N'Dongo, K. Merz, I. Ott, R. Gust and U. Schatzschneider, *Chem. Commun.*, 2008, 1798–1800.
47 H. Pfeiffer, A. Rojas, J. Niesel and U. Schatzschneider, *Dalton Trans.*, 2009, 4292–4298.
48 J. B. Matson, M. J. Webber, V. K. Tamboli, B. Weber and S. I. Stupp, *Soft Matter*, 2012, **8**, 6689–6692.
49 P. Govender, S. Pai, U. Schatzschneider and G. Smith, *Inorg. Chem.*, 2013, **52**, 5470–5478.
50 N. E. Brückmann, M. Wahl, G. J. Reiß, M. Kohns, W. Wätjen and P. C. Kunz, *Eur. J. Inorg. Chem.*, 2011, 4571–4577.
51 U. Hasegawa, A. J. van der Vlies, E. Simeoni, C. Wandrey and J. A. Hubbell, *J. Am. Chem. Soc.*, 2010, **132**, 18273–18280.
52 G. Dördelmann, H. Pfeiffer, A. Birkner and U. Schatzschneider, *Inorg. Chem.*, 2011, **50**, 4362–4367.
53 G. Dördelmann, T. Meinhardt, T. Sowik, A. Krüger and U. Schatzschneider, *Chem. Commun.*, 2012, **48**, 11528–11530.
54 M. Ma, H. Noei, B. Mienert, J. Niesel, E. Bill, M. Muhler, R. A. Fischer, Y. Wang, U. Schatzschneider and N. Metzler-Nolte, *Chem.–Eur. J.*, 2013, **19**, 6785–6790.
55 C. R. Bertozzi and E. M. Sletten, *Angew. Chem., Int. Ed.*, 2009, **48**, 6974–6998.
56 R. K. V. Lim and Q. Lin, *Chem. Commun.*, 2010, **46**, 1589–1600.
57 J. C. Jewett and C. R. Bertozzi, *Chem. Soc. Rev.*, 2010, **39**, 1272–1279.
58 P. Thirumurugan, D. Matosiuk and K. Jozwiak, *Chem. Rev.*, 2013, **113**, 4905–4979.
59 C. Bischof, T. Joshi, A. Dimri, L. Spiccia and U. Schatzschneider, *Inorg. Chem.*, 2013, **52**, 9297–9308.
60 B. W. Michel, A. R. Lippert and C. J. Chang, *J. Am. Chem. Soc.*, 2012, **134**, 15668–15671.
61 J. Wang, J. Karpus, B. S. Zhao, Z. Luo, P. R. Chen and C. He, *Angew. Chem., Int. Ed.*, 2012, **51**, 9652–9656.
62 L. Yuan, W. Lin, L. Tan, K. Zheng and W. Huang, *Angew. Chem., Int. Ed.*, 2013, **52**, 1628–1630.
63 A. J. Atkin, J. M. Lynam, B. E. Moulton, P. Sawle, R. Motterlini, N. M. Boyle, M. T. Pryce and I. J. S. Fairlamb, *Dalton Trans.*, 2011, **40**, 5755–5761.
64 S. McLean, B. E. Mann and R. K. Poole, *Anal. Biochem.*, 2012, **427**, 36–40.
65 R. Motterlini, J. E. Clark, R. Foresti, P. Sarathchandra, B. E. Mann and C. J. Green, *Circ. Res.*, 2002, **90**, e17–e24.
66 M. A. Gonzalez, M. A. Yim, S. Cheng, A. Moyes, A. J. Hobbs and P. K. Mascharak, *Inorg. Chem.*, 2011, **51**, 601–608.
67 W. Huber, R. Linder, J. Niesel, U. Schatzschneider, B. Spingler and P. C. Kunz, *Eur. J. Inorg. Chem.*, 2012, **2012**, 3140–3146.
68 D. L. Reger, J. D. Elgin, R. F. Semeniuc, P. J. Pellechia and M. D. Smith, *Chem. Commun.*, 2005, 4068–4070.
69 D. L. Reger, B. Reinecke, M. D. Smith and R. F. Semeniuc, *Inorg. Chim. Acta*, 2009, **362**, 4377–4388.
70 G. R. Fulmer, A. J. M. Miller, N. H. Sherden, H. E. Gottlieb, A. Nudelman, B. M. Stoltz, J. E. Bercaw and K. I. Goldberg, *Organometallics*, 2010, **29**, 2176–2179.
71 C. A. Parker, *Proc. R. Soc. London, Ser. A*, 1953, **220**, 104–116.
72 C. G. Hatchard and C. A. Parker, *Proc. R. Soc. London, Ser. A*, 1956, **235**, 518–536.

73 H. J. Kuhn, S. E. Braslavskyi and R. Schmidt, *Pure Appl. Chem.*, 1989, **61**, 187–210.
74 E. A. Jaffe, R. L. Nachman, C. G. Becker and C. R. Minick, *J. Clin. Invest.*, 1973, **52**, 2745–2756.
75 F. Neese, *WIREs Comput. Mol. Sci.*, 2011, **2**, 73–78.
76 A. Schaefer, H. Horn and R. Ahlrichs, *J. Chem. Phys.*, 1992, **97**, 2571–2577.
77 F. Weigend and R. Ahlrichs, *Phys. Chem. Chem. Phys.*, 2005, **7**, 3297–3305.
78 G. M. Sheldrick, Universität Göttingen, Germany, 2006.
79 O. V. Dolomanov, L. J. Bourhis, R. J. Gildea, J. A. K. Howard and H. Puschmann, *J. Appl. Crystallogr.*, 2009, **42**, 339–341.